ZunYue Huang, Zhen Luo*, SanSan Ao and YangChuan Cai

Effect of Laser Welding Parameters on Weld Bowing Distortion of Thin Plates

DOI 10.1515/htmp-2016-0153
Received July 12, 2016; accepted February 6, 2017

Abstract: Weld bowing distortions are detrimental to the assembly process, where laser process parameters such as laser power, welding speed, defocusing distance and gas flow rate play a significant role in determining the weld bowing distortion. Herein, weld bowing distortions in 1-mm-thick AA5052 aluminum were measured by the digital image correlation technique following laser welding. Two mathematical response models were developed to predict the laser weld bowing distortion according to the central composite rotatable design method. The optimized process parameters for minimum bowing distortion were obtained, and the influence of the laser process parameters on the weld bowing distortions was found.

Keywords: laser welding, weld bowing distortion, mathematical model

Introduction

Currently, there is a trend toward weight reduction in the automobile industry and aviation and aerospace fields [1]. Aluminum alloys are widely used as lightweight alloys in thin structures because of their favorable characteristics of high specific strength and absorption of failure energy. Compared with thick plates, welding deformation of thin sheets is more likely to occur [2], and especially weld bowing distortions, which are extremely unfavorable for the assembly process and adversely affect the precision of the structure. Correcting these distortions after welding becomes cumbersome and expensive. Obviously, prevention or control of the distortion during fabrication is desirable [3]. Removing the distortion during the fabrication process by providing an initial distortion in the negative direction and controlling the welding parameters are commonly used to control welding deformation [4–5], so predicting the weld bowing distortion under different welding parameters is important. Murugan and Gunaraj [5] have developed second-order quadratic mathematical models to predict the angular distortion of gas-metal-arc-welded structural steel plates. Further, Venkatesan et al. [3, 6] have developed experimental regression equations to predict the bowing and angular distortions of 409 M ferritic stainless steel after flux-cored arc welding. The aluminum alloy structures in the automobile industry and the aviation and aerospace fields are often fabricated by laser welding owing to its superior properties of high speed, high efficiency, a minimal heat-affected zone, deep penetration, and easy control with industrial robots [7–8]. However, there is no mathematical response model between the laser welding parameters and the weld bowing distortion of AA5052 aluminum alloy sheets.

In the present paper, two mathematical models were developed to establish relationships between the laser process parameters of laser power (P), welding speed (v), defocusing distance (D) and gas flow rate (G) and the weld bowing distortion of 1-mm-thick AA5052 aluminum fabricated by laser welding. The weld bowing distortion was measured by the digital image correlation technique after laser welding. Central composite rotatable design was used as an experimental analysis method to obtain the effects of the welding parameters on the weld bowing distortion, whereupon the optimized process parameters to achieve minimum bowing distortion were also obtained.

Experimental procedures

Materials

The base material used was a 1.0-mm-thick plate of aluminum alloy AA5052, whose chemical composition and mechanical properties are listed in Table 1. The sheet size used was 150 mm × 100 mm × 1 mm.

***Corresponding author: Zhen Luo,** School of Materials Science and Engineering, Tianjin University, Tianjin, China; Collaborative Innovation Center of Advanced Ship and Deep-Sea Exploration, Shanghai, China, E-mail: lz_tju@163.com
ZunYue Huang: E-mail: hzysmile@126.com, **SanSan Ao, YangChuan Cai,** School of Materials Science and Engineering, Tianjin University, Tianjin, China

Table 1: Chemical composition and mechanical properties of AA5052.

AA5052 (%)	Mg	Si	Cu	Zn	Mn	Cr	Fe	Al
	2.5	0.23	0.08	0.09	0.08	0.26	0.36	Remained
AA5052 (MPa)	σ_b				$\sigma_{0.2}$			
	221				86			

σ_b means ultimate tensile strength
$\sigma_{0.2}$ means nominal yield strength

Design matrix of experiments

The central composite rotatable design was used in this work, which is a response surface method. This is an experiment analysis method based on mathematical statistics and can be used to realize factor optimization by establishing a regression relationship between the factors and the response value, whereby the effect law and the effect significance of each factor can be obtained [9]. In the central composite rotatable design, there are three kinds of points: center points, star points and factorial design points. Herein, a five-level, four-factor, and central composite rotatable factorial design consisting of 36 sets of numerical conditions was chosen for ascertaining the relationship between the response (weld bowing distortion) and the variables (welding parameters). These 36 sets of numerical conditions comprised 16 factorial design points, 12 center points and 8 star points. The welding variables of the intermediate level (0) constituted the 12 center points, while the welding variables of the lowest (−2) or highest (+2) levels along with the other three variables of the intermediate level constituted the 8 star points. Before the central composite rotatable factorial design was conducted, trial experiments were performed to determine the working ranges of the parameters. The selection criteria used for these parameters were that neither external nor internal defects are formed in the weld. The determined working ranges are listed in Table 2 and the actual central composite rotatable design of the matrix is shown in Table 3.

Table 2: Welding parameters and their levels used in this study.

Parameters	Levels				
	−2	−1	0	1	2
Welding power (W)	900	1,000	1,100	1,200	1,300
Welding speed (mm/s)	5	6	7	8	9
Defocusing distance (mm)	−2	−1	0	1	2
Gas flow rate (L/min)	5	10	15	20	25

Table 3: Central composite rotatable design matrix.

No.	Welding parameters			
	Laser power P (mm)	Welding speed v (mm/s)	Defocusing distance D (mm)	Gas flow rate G (L/min)
1	1,000	6	−1	10
2	1,200	6	−1	10
3	1,000	8	−1	10
4	1,200	8	−1	10
5	1,000	6	1	10
6	1,200	6	1	10
7	1,000	8	1	10
8	1,200	8	1	10
9	1,000	6	−1	20
10	1,200	6	−1	20
11	1,000	8	−1	20
12	1,200	8	−1	20
13	1,000	6	1	20
14	1,200	6	1	20
15	1,000	8	1	20
16	1,200	8	1	20
17	900	7	0	15
18	1,300	7	0	15
19	1,100	5	0	15
20	1,100	9	0	15
21	1,100	7	−2	15
22	1,100	7	2	15
23	1,100	7	0	5
24	1,100	7	0	25
25	1,100	7	0	15
26	1,100	7	0	15
27	1,100	7	0	15
28	1,100	7	0	15
29	1,100	7	0	15
30	1,100	7	0	15
31	1,100	7	0	15
32	1,100	7	0	15
33	1,100	7	0	15
34	1,100	7	0	15
35	1,100	7	0	15
36	1,100	7	0	15

Measurement for weld bowing distortion

Figure 1 shows the welding procedure and the weld bowing distortion measurement apparatus. The laser source used was a 2 kW continuous wave Nd:YAG laser (JK2003SM) controlled by a multi-axis computer numeric control (CNC) console (TDJG-1). Further, argon gas with 99.99 % purity was used as the shielding gas. To research the intuitive deformation behavior of the thin plates, all of the specimens were welded without any external restraint. A more detailed description of the methods

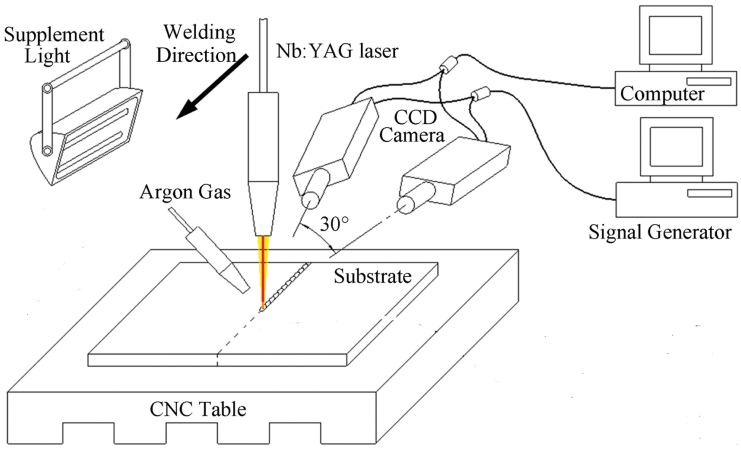

Figure 1: Schematic of experimental apparatus.

used can be found in a previous study researching in-plane deformation behavior [10]. The weld bowing distortion of 1-mm-thick AA5052 aluminum was measured by the digital image correlation technique. The images before and after welding were acquired by two charge-coupled device (CCD) cameras with an intersection angle of 30 degrees. The deformation was measured by matching two corresponding points on two images using the VIC-3D™ software. A random black-on-white speckle pattern was sprayed on the surface of all of the specimens before welding, as shown in Figure 2. Figure 3 shows the image-matching procedure, wherein the image acquired before welding is set as the reference image and those acquired after welding are the deformation images. A small subset area of the image is tracked as the specimen moves and deforms. To perform this tracking, the subset area is shifted until the pattern in the deformed image matches that in the reference image as closely as possible, where this match is calculated as the total difference in the gray levels at each point. A practical zero-mean normalized sum of squared differences (ZNSSD) criterion is used to evaluate the similarity between the reference subsets and the deformation subsets [11–12], which is given as

$$C_{ZNSSD(P)} = \sum_{i=-M}^{M}\sum_{j=-M}^{M} \left[\frac{f(x_i,y_j)-f_m}{\sqrt{\sum_{i=-M}^{M}\sum_{j=-M}^{M}[f(x_i,y_i)-f_m]}^{2}} - \frac{g\left(x_i',y_j'\right)-g_m}{\sqrt{\sum_{i=-M}^{M}\sum_{j=-M}^{M}\left[g\left(x_i',y_j'\right)-gm\right]}^{2}}\right], \quad (1)$$

where **P** is the desired deformation vector depicting the shape and position of the deformation subset relative to the reference subset; and $f(x_i, y_j)$ and $g\left(x_i', y_j'\right)$ are the grayscale intensities at the coordinates of (x_i, y_j) in the reference subset and $\left(x_i', y_j'\right)$ in the deformation subset, respectively. The mean intensity values of the reference and deformation subsets are given as

$$f_m = \frac{1}{(2M+1)^2}\sum_{i=-M}^{M}\sum_{i=-M}^{M}\left[f(x_i,y_j)\right], \quad (2)$$

$$g_m = \frac{1}{(2M+1)^2}\sum_{i=-M}^{M}\sum_{i=-M}^{M}\left[g(x_i',y_j')\right]. \quad (3)$$

Figure 4 shows the three-dimensional (3D) deflection contour of the plate, as well as the weld bowing distortion chosen for evaluation by the digital image correlation technique. The measured weld bowing distortion is obtained from the difference between the maximum and minimum deflection values.

Figure 2: Random black-on-white speckle patterns sprayed on the surfaces of all specimens.

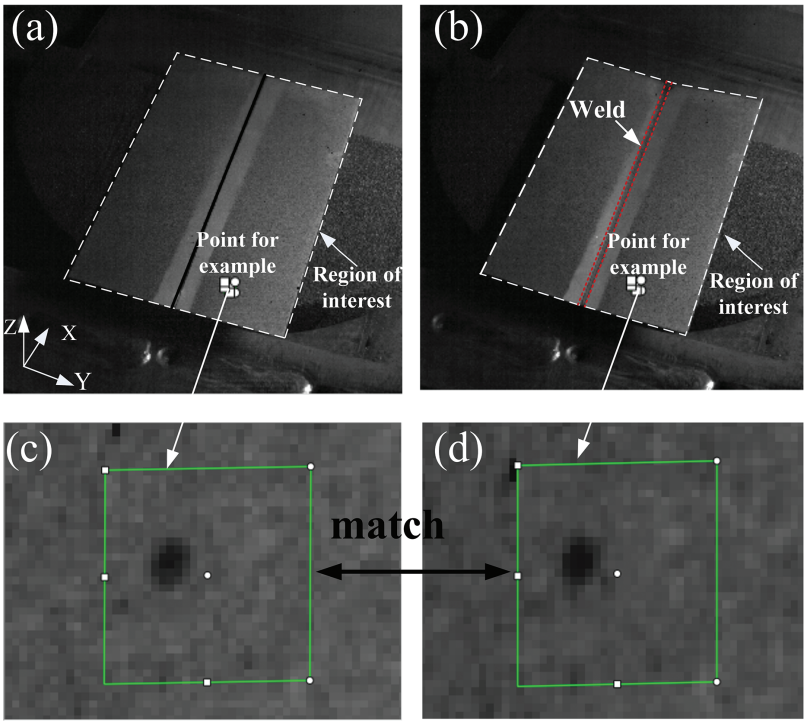

Figure 3: Match procured between the reference and deformation images: (a) reference image, (b) deformation image, (c) and (d) are the magnified points on (a) and (b), respectively.

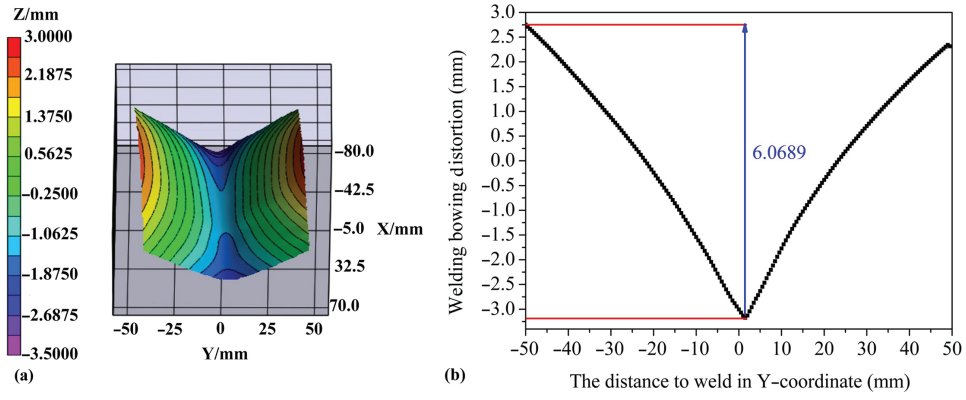

Figure 4: 3D deflection contour of the plate and the evaluated weld bowing distortion (laser power, $P = 1000$ W; welding speed, $v = 6$ mm/s; defocus distance, $D = -1$ mm; gas flow rate, $G = 10$ L/min).

Results and discussion

The measured weld bowing distortion for the central composite rotatable design matrix is shown in Table 4. The deflection is symmetric, which correlates with what is observed in Figure 3. The shape of the welded specimen is a convex–concave–convex saddle, which is consistent with previous research [13]. The maximum deflection is at the central zone of the plate edge along the welding direction, while the minimum deflection values are at the two ends of the weld. The measured weld bowing distortion is obtained from the difference between these maximum and minimum deflection values.

Table 4: Measured weld bowing distortion for central composite rotatable design matrix.

No.	Weld bowing distortion *WD* (mm)	No.	Weld bowing distortion *WD* (mm)
1	6.06894	19	5.92253
2	6.16096	20	4.92502
3	5.60902	21	6.20625
4	5.96223	22	5.42988
5	5.55055	23	5.6234
6	6.14424	24	5.4612
7	5.43886	25	5.60318
8	5.59928	26	5.55436
9	5.3753	27	5.62416
10	5.83376	28	5.58557
11	5.29193	29	5.53955
12	5.70418	30	5.59124
13	5.19701	31	5.59705
14	5.67756	32	5.49876
15	4.96565	33	5.5603
16	5.47836	34	5.52336
17	5.4513	35	5.56074
18	5.99669	36	5.54223

Development and selection of the response model

Using a module involving the response surface method included in the Design-Expert software, parameter optimization and a subsequent analysis based on the central composite rotatable design method can be implemented conveniently and effectively. According to the characteristics of the substituted data, the optimum order of the response model is automatically suggested, in which the significance of each order in the response model is evaluated according to the *F*-test. Table 5 shows the sequential sums of squares for the distortion mode, where it can be seen that terms of increasing complexity contribute to the total model. The model hierarchy is described as: (1)'Linear versus Mean': the significance of adding the linear terms to the mean; (2)'2FI versus Linear': the significance of adding the two-factor interaction terms to the mean and linear terms already in the model; (3)'Quadratic versus 2FI': the significance of adding the quadratic (squared) terms to the mean, linear, and two-factor interaction terms already in the model; and (4)'Cubic versus Quadratic': the significance of the cubic terms beyond all other terms. For each source of terms (linear, etc.), we examine the probability ("Prob > *F*") to see if it falls below 0.05, which is the criteria used to choose models. The probability ("Prob > *F*") falling below 0.05 signifies that the source of the terms is significant. Here, the linear and quadratic and cubic models meet these requirements. However, the cubic model is aliased, which means that the cubic terms are not useful for modeling purposes. Therefore, two methods are suggested by the software. In addition, in the model summary statistics shown in Table 6 exhibiting the 'standard deviation', '*R*-Squared', 'Adjusted *R*-squared' and 'Press' values, the program automatically underlines the 'Suggested' model. The criteria for choosing models focus on the model that maximizes the 'Adjusted *R*-Squared' and reduces the 'standard deviation'. The data in Tables 5 and 6 indicate that the linear and quadratic models are statistically appropriate for the weld bowing distortion and are suitable for further analysis in this investigation. Therefore, we used the linear model and the quadratic model to respectively establish the relationship between the welding parameters and the weld bowing distortion of the welded sheets and to ultimately predict the weld bowing distortion and the corresponding optimum combination of welding parameters. The linear model focuses on the direct impact of the individual factors upon the results and the quadratic model focuses on the impact of interaction between several factors upon the results.

Table 5: Sequential sums of squares for the distortion model.

Source	Sum of squares	df	Mean square	*F* value	*P*-value Prob > *F*	
Mean versus Total	1,131.81	1	1,131.81			
Linear versus Mean	2.35	4	0.59	29.17	<0.0001	Suggested
2FI versus Linear	0.075	6	0.012	0.57	0.7531	
Quadratic versus 2FI	0.22	4	0.055	3.53	0.0237	Suggested
Cubic versus Quadratic	0.28	8	0.035	8.66	0.0004	
Residual	0.052	13	3.991×10^{-1}			
Total	1,134.78	36	31.52			

Table 6: Model summary statistics for the distortion model.

Source	Standard deviation	*R*-squared	Adjusted *R*-squared	Press	
Linear	0.14	0.7901	0.7630	0.94	Suggested
2FI	0.15	0.8152	0.7413	1.43	
Quadratic	0.13	0.8895	0.8158	1.82	Suggested
Cubic	0.063	0.9825	0.9530	5.39	Aliased

Linear model

For a mathematical response model involving four factors, the linear response y can be described in the form:

$$y = a_0 + \sum^{a_i} x_i, \tag{4}$$

where a_O is the intercept term, a_i is the linear term, and x_i is the factor.

In the present study, the response (i. e. weld bowing distortion (WD)) is a function of laser power (P), welding speed (v), defocusing distance (D) and gas flow rate (G); therefore the equation can be expressed as

$$WD = a_0 + a_1P + a_2v + a_3D + a_4G. \tag{5}$$

The Design-Expert software is used to calculate linear model coefficients via substituting experimental results of the measured weld bowing distortion shown in Table 4. The coefficients are calculated by fitting a linear regression relationship between the factors and the response value. The fitting coefficients are the linear regression coefficients based on multiple linear regression theory. Therefore, the equation can be expressed as:

$$WD = 5.27316 + 1.73087 \times 10^{-3}P - 0.16474v - 0.14615D - 0.027789G. \tag{6}$$

The accuracy of the developed response model can be determined through variance analysis and residual analysis [9, 14–15]. Table 7 shows the variance analysis of the linear response model for the weld bowing distortion. The model gives a highly significant F-value, demonstrating that the model adequately represents the actual relationship between the response and the variables. Any model term with $p<0.05$ is significant, so P, v, D and G all are significant model terms. Figure 5 shows

Table 7: Variance analysis of the linear model.

Source	Sum of squares	df	Mean square	*F*-value	*p*-value Prob > *F*	Significant
Model	2.35	4	0.59	29.17	<0.0001	–**
Laser power(*P*)	0.72	1	0.72	35.75	<0.0001	–**
Welding speed (*v*)	0.65	1	0.65	32.39	<0.0001	–**
Defocusing distance (*D*)	0.51	1	0.51	25.49	<0.0001	–**
Gas flow rate (*G*)	0.46	1	0.46	23.04	<0.0001	–**
Residual	0.62	31	0.020			
Lack of fit	0.61	20	0.030			
Pure error	0.015	11	1.322×10^{-3}			
Cor total	2.97	35				

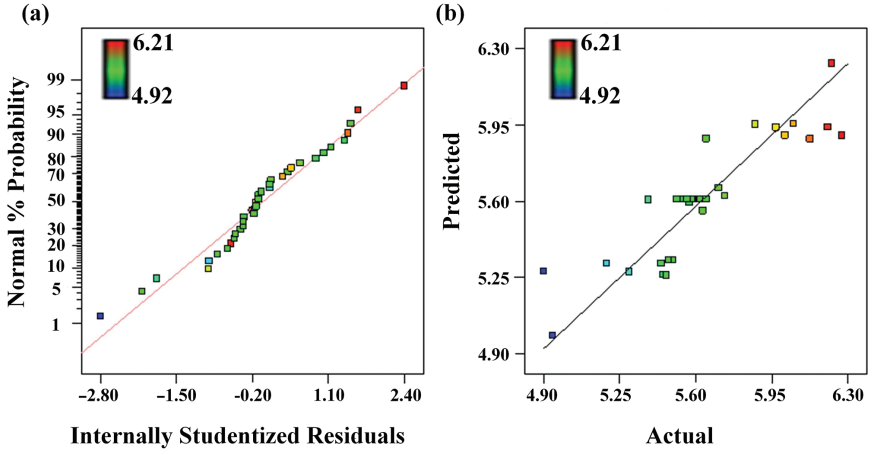

Figure 5: Linear model. (a) Normal probability plot of the residuals and (b) plot of actual versus predicted weld bowing distortion.

the normal distribution probability of residuals and the comparison of experimental results versus predicted results, which exhibit a high accuracy of the developed mathematical response model.

Quadratic model

The quadratic response y is described in the form of the equation:

$$y = b_0 + \sum b_i x_i + \sum b_{ij} x_i x_j + \sum b_{ii} x_i^2, \tag{7}$$

where b_0 is the intercept term, b_i is the linear term, b_{ii} is the quadratic term and b_{ij} is the interaction term.

In the present study, the response (i. e. WD) is a function of laser power (P), welding speed (v), defocusing distance (D) and gas flow rate (G); therefore, the equation can be expressed as:

$$WD = b_0 + b_1 P + b_2 V + b_3 D + b_4 G + b_{12} PV + b_{13} PD + b_{14} PG + b_{23} VD + b_{24} VG + b_{34} DG + b_{11} P^2 + b_{22} V^2 + b_{33} D^2 + b_{44} G^2. \tag{8}$$

Similar to the determination of coefficients in the linear model, the Design-Expert software is also used to calculate the quadratic model coefficients via substituting experimental results of the measured weld bowing distortion shown in Table 4. The coefficients are calculated by fitting a quadratic regression relationship between the factors and the response value. The fitting coefficients are the regression coefficients based on multiple nonlinear regression theory. By applying multiple regression analysis on the design matrix and the response values, the following second-order polynomial equation is established:

$$\begin{aligned} WD = {} & 9.662 - 7.501 \times 10 - 3P + 0.338v - 0.382D - 0.171G \\ & - 1.163 \times 10 - 4Pv + 2.696 \times 10 - 4PD + 8.308 \times 10 \\ & - 5PG - 0.013vD + 8.397 \times 10 - 3vG + 2.270 \times 10 \\ & - 3DG + 4.000 \times 10 - 6P^2 - 0.035v^2 + 0.064D^2 \\ & - 2.169 \times 10 - 4G^2. \end{aligned} \tag{9}$$

Table 8 shows the variance analysis of the quadratic model for the weld bowing distortion. The model gives a highly significant F-value, demonstrating that the model adequately represents the actual relationship between the response and the variables. Any model term with $p < 0.05$ is significant, so P, v, D and G all are significant model terms. Figure 6 shows the normal distribution probability of residuals and the comparison of experimental results versus predicted results, which exhibit a high accuracy of the developed mathematical response model.

Table 8: Variance analysis of the quadratic model.

Source	Sum of squares	df	Mean square	F-value	p-value Prob > F	Significant
Model	2.64	14	0.19	12.07	<0.0001	–**
Laser power (P)	0.72	1	0.72	46.00	<0.0001	–**
Welding speed (v)	0.65	1	0.65	41.67	<0.0001	–**
Defocusing distance (D)	0.51	1	0.51	32.79	<0.0001	–**
Gas flow rate (G)	0.46	1	0.46	29.64	<0.0001	–**
$P \times v$	2.165×10^{-3}	1	2.165×10^{-3}	0.14	0.7135	–*
$P \times D$	0.012	1	0.012	0.74	0.3981	–*
$P \times G$	0.028	1	0.028	1.77	0.1981	–*
$v \times D$	2.906×10^{-3}	1	2.906×10^{-3}	0.19	0.6708	–*
$v \times G$	0.028	1	0.028	1.80	0.1935	–*
$G \times D$	2.062×10^{-3}	1	2.062×10^{-3}	0.13	0.7201	–*
P^2	0.051	1	0.051	3.28	0.0847	–*
v^2	0.039	1	0.039	2.52	0.1277	–*
G^2	0.13	1	0.13	8.26	0.0091	–*
D^2	9.407×10^{-4}	1	9.407×10^{-4}	0.060	0.8086	–*
Residual	0.33	21	0.016			
Lack of fit	0.31	10	0.031			
Pure error	0.015	11	1.322×10^{-3}			
Cor total	2.97	35				

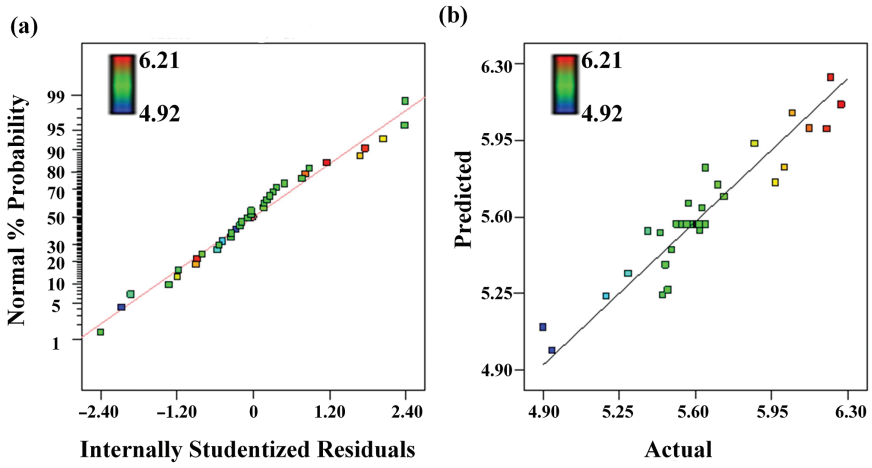

Figure 6: Quadratic model: (a) normal probability plot of the residuals and (b) plot of actual versus predicted weld bowing distortion.

Effect of welding parameters on weld bowing distortion

The effects of the welding parameters on the weld bowing distortion were predicted by the linear and quadratic models. Figure 7 shows the direct impact of individual factors on the weld bowing distortion as predicted by the linear model. Figures 8 and 9 show 3D response surface graphs and contour plots based on the quadratic model by considering two of the four parameters in the middle level and the other two parameters as variables. This effectively focuses on the effect that an interaction between several factors has on the results.

Figure 7 shows that the weld bowing distortion gradually increases with the laser power, while it decreases with increasing welding speed, defocusing distance and gas flow rate. Figures 8 and 9 show the interaction effect of several factors on the weld bowing distortion, which reveals that the weld bowing distortion is low at a high welding speed, a low laser power, a positive defocusing distance and a large gas flow rate. The parameter values producing a minimum weld bowing distortion in the working range is a laser power of 900 W, a welding speed of 9 mm/s, a defocusing distance of 2 mm and a gas flow rate of 25 L/min. The effect of the parameters on the weld bowing distortion is related closely to the

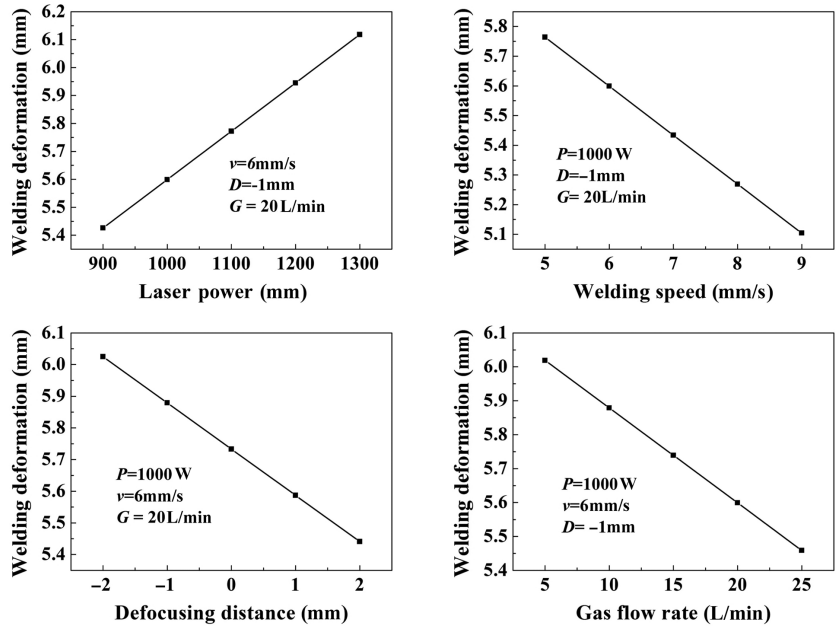

Figure 7: Direct impact of individual factors on the weld bowing distortion as predicted by linear model.

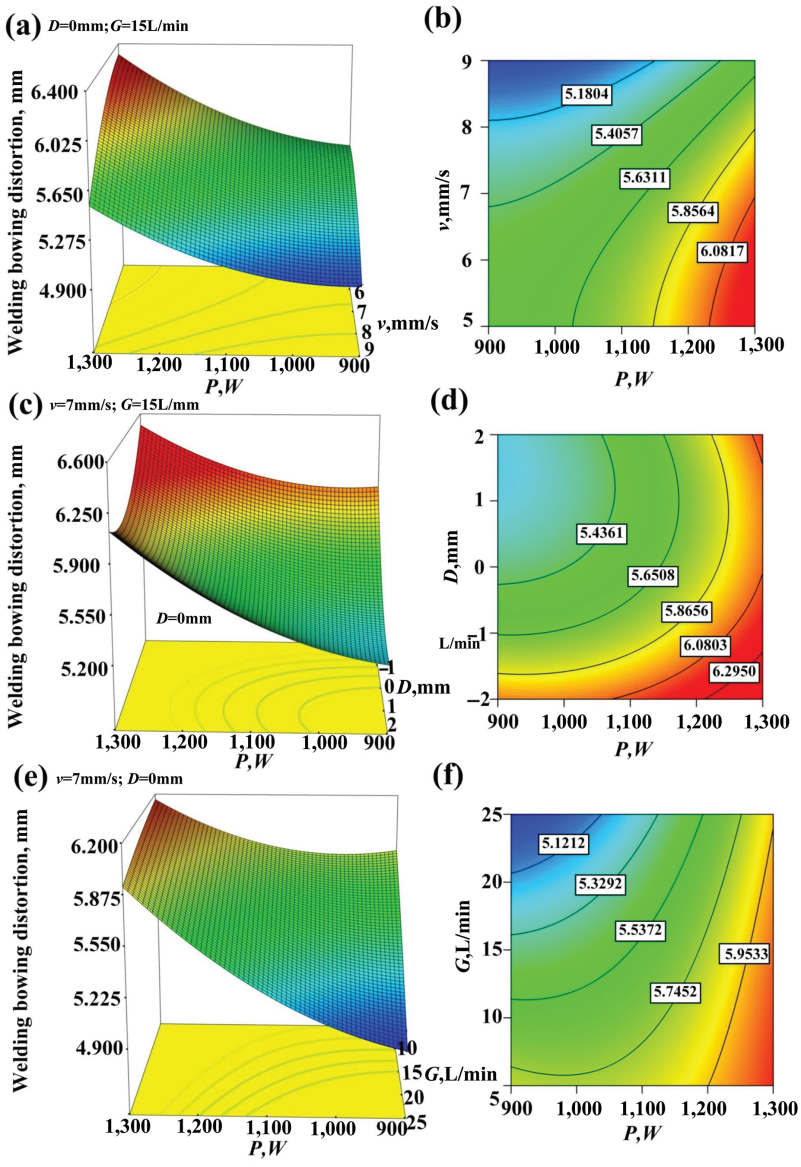

Figure 8: 3D response surface graphs and contour plots based on the quadratic model: (a), (c), (e) response surface graphs demonstrating the interaction effects of laser power with the other three welding parameters; (b), (d), (f) contour plots of (a), (c), (e), respectively.

formation of the distortion. First, the weld metal is heated to melting temperatures by the laser, causing the temperature of the weld metal at the plate area near the laser to be high and that of the areas far away from the laser to be low. This temperature gradient on the plate results in the thermally expanding weld metal at the high-temperature areas to be constrained by the surrounding low-temperature metal. Therefore, the weld metal is subjected to a thermal compressive stress σ_P while the metal far away from the weld is subjected to a tensile thermal stress σ_t, as shown in Figure. 10(a). The direction of the arrow represents the force direction in Figure 10. As heating continues, the material yield limit R_{el} decreases with increasing temperature, and when σ_P exceeds R_{el} the thermal expansion transforms into an internal compressive plastic strain. In the cooling process of the welding, the compressive plastic strain causes the weld metal to shrink, whereupon the weld metal is subjected to a residual tensile stress σ_{rt} and the metal far away from the weld is subjected to residual compressive stress σ_{rP}, as shown in Figure 10(b). Finally, Figure 10(c) shows the plate after the weld bowing distortion occurs.

The laser power and welding speed have direct effects on the heat input (*HI*), where the formula is given as [16]

$$HI = P/v, \tag{10}$$

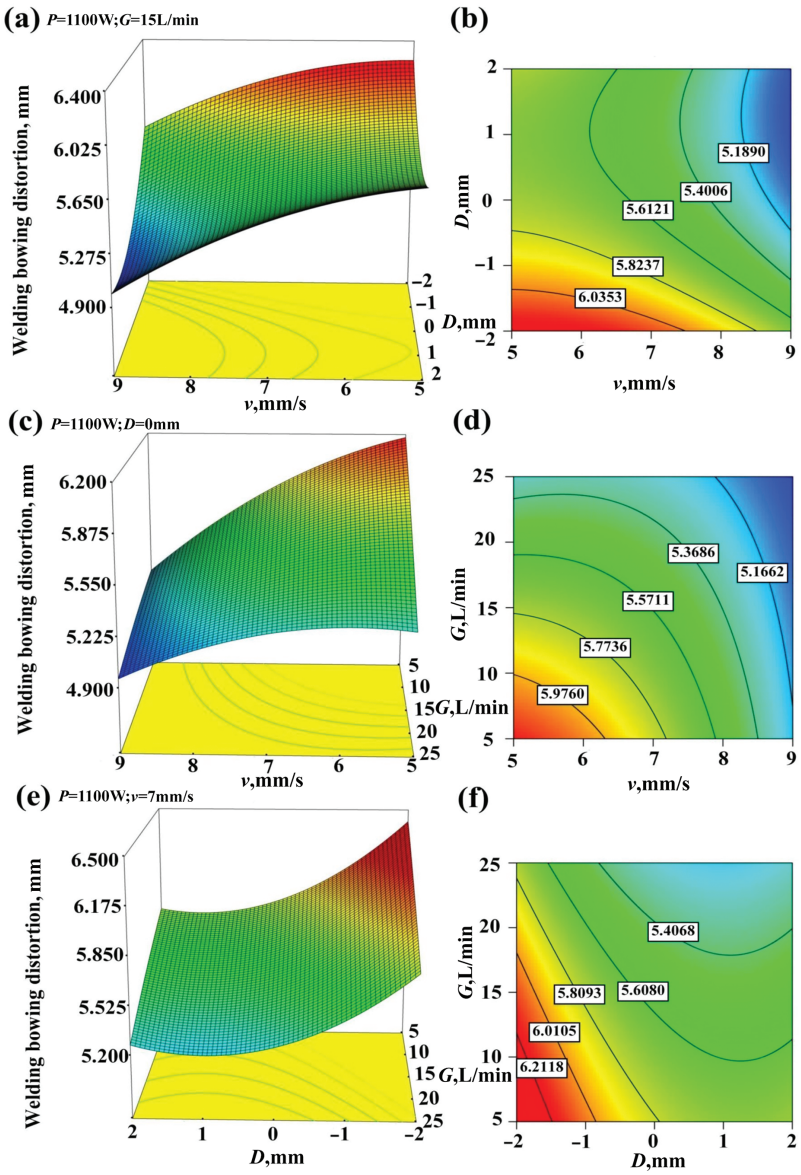

Figure 9: 3D response surface graphs and contour plots based on the quadratic model: (a), (c), (e) response surface graphs demonstrating the interaction effects of the welding speed, defocusing distance and gas flow rate; (b), (d), (f) contour plots of (a), (c), (e), respectively.

where P is the laser power and v is the welding speed.

In this relationship, a larger laser power and smaller welding speed increase the heat input, whereupon the temperature of the weld metal increases and the volume of the molten metal also increases. This causes the degree of thermal expansion to be greater, so the weld bowing distortion is also bigger. Similarly, the defocusing distance has a significant influence on the energy density. When the defocusing distance is negative, the energy density in the weld keyhole is greater than that of the weld surface and the temperature of the weld metal is therefore higher. This causes the unbalanced temperature gradient to increase, inducing a more extreme weld bowing distortion [17]. Finally, the gas flow rate affects the weld bowing distortion in two aspects: First, the cold Ar gas flew out of the nozzle has a cooling effect on the melted welding pool and surrounding area, and the gas temperature increases because of the heating exchange. Second, the heated gas was blown away from the welding pool area and towards the weld tail, and reduced the weld tail cooling rate due to its higher than ambient temperature. Hence, higher gas flow rate would result in more cooling effect at the welding pool area and lower cooling rate at the weld tail. Therefore, a greater gas flow rate results in less temperature gradient between the welding pool and the weld tail, which inhibits the

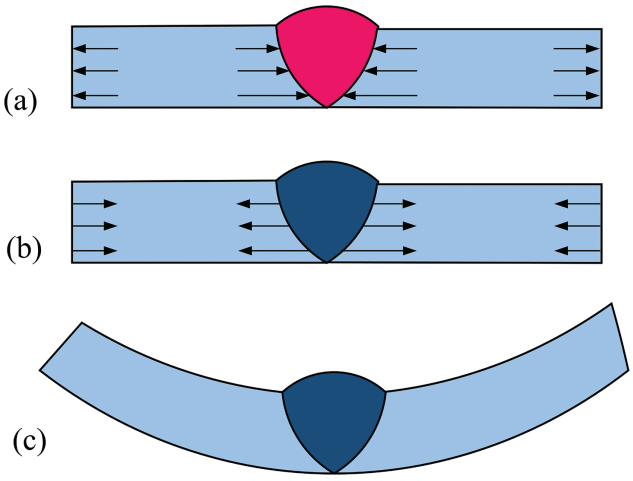

Figure 10: Schematic for the formation of the weld bowing distortion. (a) Force diagram of the weldment during the heating process of welding. (b) Force diagram of the weldment during the cooling process of the welding. (c) The plate exhibiting weld bowing distortion.

formation of the weld bowing distortion. Moreover, Venkatesan et al. have revealed that the weld bowing distortion of 409 stainless steel after flux-cored arc welding is closely related to the weld bead width, wherein the plates with wider bead widths usually have larger welding deformations [3]. Shen Xiaolong has given an estimation formula for the weld width in continuous laser welding that reveals that the welding parameters have a significant influence on the weld bead width [17]. The formula is given as:

$$b = 0.48kP/(vdKT_m), \tag{11}$$

where P is laser power; d is the laser spot diameter (related to the defocusing distance); v is the welding speed and k, K and T_m are the thermal diffusivity, thermal conductivity and melting temperature, respectively.

Figures 11–14 show the weld stereomicroscope images under different laser powers, welding speeds, defocusing distances and gas flow rates, respectively. Tables 9–12 give

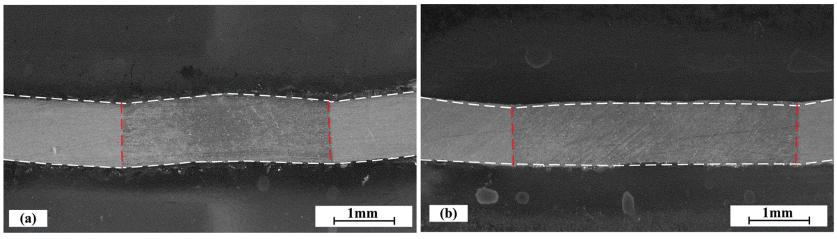

Figure 11: Weld stereomicroscope images under different laser powers of (a) sheet No. 9 and (b) sheet No. 10.

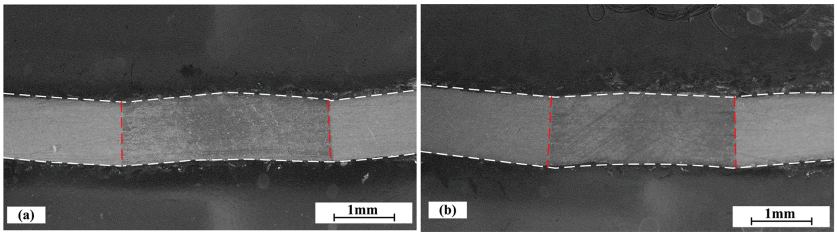

Figure 12: Weld stereomicroscope images under different welding speeds of (a) sheet No. 9 and (b) sheet No. 11.

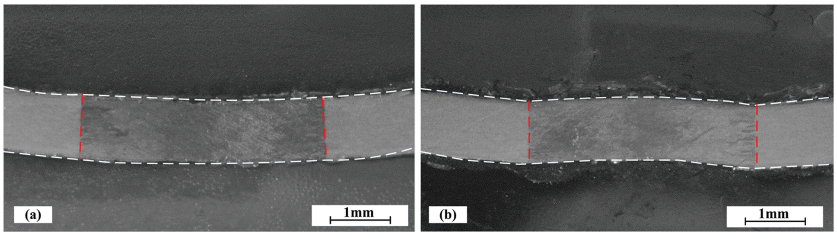

Figure 13: Weld stereomicroscope images under different defocusing distance of (a) sheet No. 1 and (b) sheet No. 5.

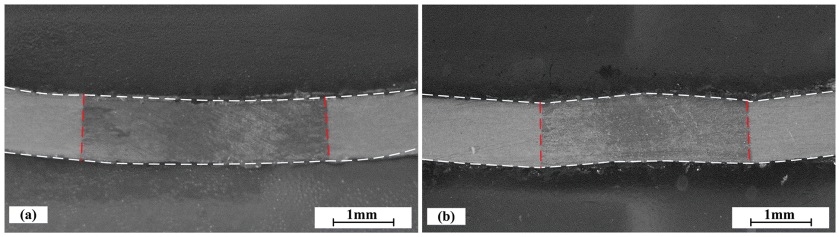

Figure 14: Weld stereomicroscope images under different gas flow rates of (a) sheet No. 1 and (b) sheet No. 9.

the weld bead width and welding parameters corresponding to Figures 11–14, respectively. The weld beads width increases under a greater laser power, smaller welding speed, smaller defocusing distance and smaller gas flow rate, and the weld bowing distortion is larger. Therefore, the AA5052 weld bowing distortion during the laser welding process is also related to the weld bead width, which is consistent with previous studies [3]. The relationship can be understood in that a wider weld bead creates a bigger volume of molten metal and thus more heat energy absorbed. Therefore, during the laser welding process, the degree of thermal expansion is greater, so the weld bowing distortion is bigger.

Table 9: Welding parameters and bead width corresponding to Figure 11.

No.	No. 9	No. 10
Laser power (W)	1,000	1,200
Welding speed (mm/s)	6	6
Defocusing distance (mm)	−1	−1
Gas flow rate (L/min)	20	20
Weld bead width (mm)	3.53	4.84
Welding bowing distortion (mm)	5.375	5.834

Table 10: Welding parameters and bead width corresponding to Figure 12.

No.	No. 9	No. 11
Laser power (W)	1,000	1,000
Welding speed (mm/s)	6	8
Defocusing distance (mm)	−1	−1
Gas flow rate (L/min)	20	20
Weld bead width (mm)	3.53	3.12
Welding bowing distortion (mm)	5.375	5.292

Table 11: Welding parameters and bead width corresponding to Figure 13.

No.	No. 1	No. 5
Laser power (W)	1,000	1,000
Welding speed (mm/s)	6	6
Defocusing distance (mm)	−1	1
Gas flow rate (L/min)	10	10
Weld bead width (mm)	4.15	3.88
Welding bowing distortion (mm)	6.069	5.551

Table 12: Welding parameters and bead width corresponding to Figure 14.

No.	No. 1	No. 9
Laser power *(W)*	1,000	1,000
Welding speed *(mm/s)*	6	6
Defocusing distance (mm)	−1	−1
Gas flow rate (L/min)	10	20
Weld bead width (mm)	4.15	3.53
Welding bowing distortion (mm)	6.069	5.375

Conclusion

(1) Two mathematical relationships (linear and quadratic models) are developed between the weld bowing distortion and the welding parameters, which are used to predict the weld bowing distortion of laser-welded AA5052 aluminum alloy thin sheets using central composite rotatable factorial design.

(2) The laser power, welding speed, defocusing distance and gas flow rate are found to be the most significant factors affecting the weld bowing distortion. The distortion increases as the laser power increases and decreases as the welding speed, defocusing distance and gas flow rate increase. The minimum weld bowing distortion in the working range is found at a laser power of 900 W, a welding speed of 9 mm/s, a defocusing distance of 2 mm and a gas flow rate of 25 L/min.

(3) The weld bowing distortion of laser-welded AA5052 aluminum alloy thin sheets is also related to the weld bead width, where a larger weld bowing distortion typically corresponds to a wider weld bead width.

Funding: This research is supported by National Nature Science Foundation of China (grant 51275342, and grant 51275338) and Specialized Research Fund for the Doctoral Program of Higher Education (grant 20130032110004).

References

[1] M.V. Venkatesan, N. Murugan, B.M. Prasad and A. Manickavasagam,. J. Iron Steel. Res. Int., 20 (2013) 71–78.
[2] L.C. Tsai, S.C. Park and W.T. Cheng, Weld. J., 78 (1999) 156-s.
[3] H. Huang, J. Wang, L. Li and N. Ma, J. Mater. Process. Tech., 227 (2016) 117–128.
[4] C.A. Widener, J.E. Talia, B.M. Tweedy and D.A. Burford, Proceedings of the 6th International Symposium on Friction Stir Welding, Montreal, Canada, October, 2006.
[5] J.C. Wang, X.Q. Yin and H. Murakawac, J. Mater. Process. Tech., 213 (2013) 1447–1458.
[6] V.V. Murugan and V. Gunaraj, Weld. J., 11 (2005) 165–171.
[7] J. Sun, X. Liu, Y. Tong and D. Deng, Mater. Des., 63 (2014) 519–530.
[8] S.L.C. Ferreira, R.E. Bruns, H.S. Ferreira, G.D. Matos, J.M. David, G.C. Brandão, E.G.P. Da Silva, L.A. Portugal, P.S. Dos Reis, A.S. Souza and W.N.L. Dos Santos, Anal. Chim. Acta, 597 (2007) 179–186.
[9] B. Pan, H. Xie and Z. Wang, Appl. Opt., 49 (2010) 5501–5509.
[10] A.K. Sinha, D.Y. Kim and D. Ceglarek, Opt. Lasers Eng., 51 (2013) 1143–1152.
[11] M.V. Venkatesan and N. Murugan, J. Eng. Sci. Tech., 9 (2014) 106–121.
[12] X.L. Shen. The research on laser welding quality of high strength steel. Master thesis, Hunan University, (2006).
[13] W. Chen, P. Ackerson and P. Molian, Mater. Des., 30 (2009) 245–251.
[14] M. Shibahara, K. Yamaguchi, T. Onda, S. Itoh and K. Masaoka, Weld. Int., 26 (2012) 612–620.
[15] L. Liu, S. Hu, J. Shen and X. Wei, Chinese J. Lasers, 42 (2015) 0203005.
[16] J.Q. Li and H.J. Liu, Int. J. Adv. Manuf. Tech., 76 (2015) 1469–1478.
[17] B. Pan, D. Wu and L. Yu, Appl. Opt., 51 (2012) 4409–4419.